IJE TRANSACTIONS C: Aspects Vol. 37 No. 09, (September 2024) 1832-1846

International Journal of Engineering

Journal Homepage: www.ije.ir

A Lattice-adaptive Model for Solving Acoustic Wave Equations Based on Lattice Boltzmann Method

A. Shahriari[a, b], S. A. Mirbozorgi*[a], S. Mirbozorgi[c]

[a] *Mechanical Engineering Department, University of Birjand, Birjand, Iran*
[b] *Mechanical Engineering Department, University of Zabol, Zabol, Iran*
[c] *Electrical and Computer Engineering Department, University of Alabama at Birmingham, Birmingham, USA*

PAPER INFO

Paper history:
Received 17November 2023
Received in revised form 02 April 2024
Accepted 10 April 2024

Keywords:
Chapman-Enskog Expansion
Lattice-Boltzmann Method
Analytical Solution
Acoustic Wave Propagation
Lattice Structure

ABSTRACT

This paper addresses the need for an efficient and adaptable approach to solve linear acoustic wave equations in the lattice Boltzmann method (LBM). A novel lattice-adaptive model is introduced, derived through a Chapman–Enskog analysis, which utilizes a single relationship for the equilibrium distribution function across all lattice structures. The intended derivation begins by considering a standard equilibrium distribution function with unknown coefficients. By selecting the displacement of the acoustic wave as the zero-order microscopic moment, accurate recovery of the macroscopic wave equation is ensured. Unlike existing methods, the model simplifies the complexity associated with equilibrium distribution functions and offers greater versatility. The model is validated through extensive benchmark testing on one and two-dimensional wave propagation problems. Results demonstrate excellent agreement with analytical solutions, with maximum root mean square errors of 10^{-3} (<0.1% error) and minimum errors of 10^{-6} (<0.0001% error), indicating high predictive accuracy (>99.9%). Additionally, the model exhibits second-order spatial accuracy, with the relative error norm E_2 displaying slopes close to 2, signifying a spatial accuracy of second order. The numerical simulations show a decrease in errors as the mesh size becomes more refined.

***doi**: 10.5829/ije.2024.37.09c.13*

Graphical Abstract

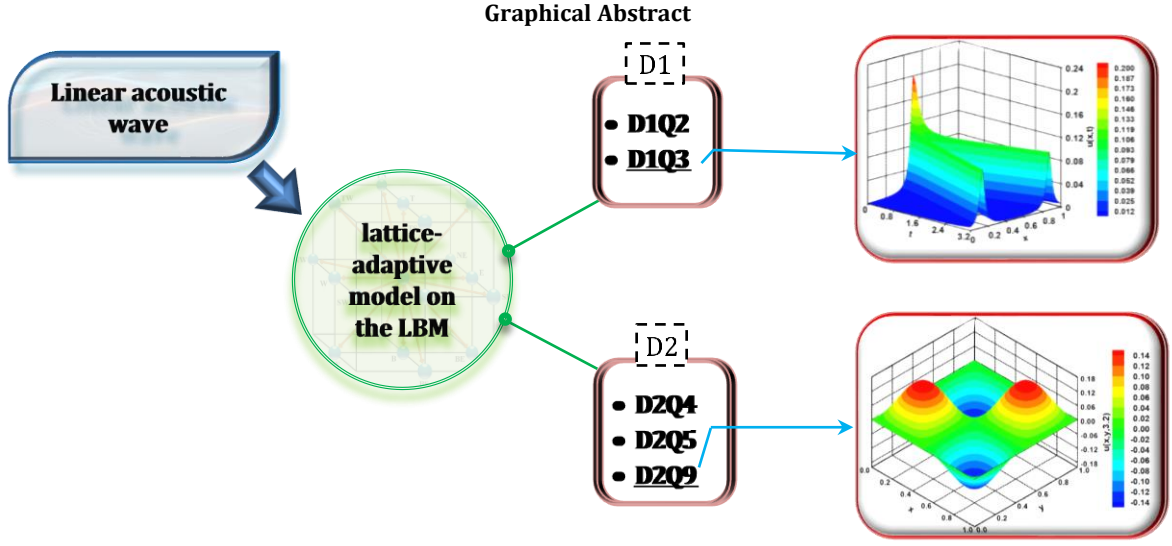

*Corresponding author email: samirbozorgi@birjand.ac.ir (S. A. Mirbozorgi)

Please cite this article as: Shahriari A, Mirbozorgi SA, Mirbozorgi S. A Lattice-adaptive Model for Solving Acoustic Wave Equations Based on Lattice Boltzmann Method. International Journal of Engineering, Transactions C: Aspects. 2024;37(06):1832-46.

1. INTRODUCTION

The wave propagation phenomenon is a transient problem that attracts considerable attention in many disciplines of science and engineering. The precise and effective solution of wave propagation is an important issue in numerous fields such as fluid dynamics, ocean physics, acoustics, natural phenomena, electromagnetics, wireless communication networks, etc. (1-6). Moreover, the ability to accurately model wave propagation phenomena has significant implications for practical applications such as the design of efficient communication networks, the prediction of natural disasters, and the development of advanced sensing technologies (4, 7).

The investigation of wave propagation in fluid media by studying wave problems has been pursued by two different methods. The first method involves the direct solution of the fluid conservation equations, namely the Navier-Stokes equations (7-11). The second method involves the solution of the simplified and combined fluid conservation equations, commonly referred to as wave equation-based models (12-16). The wave equation, a hyperbolic partial differential equation, is essential for describing wave propagation in a variety of systems. In recent decades, researchers have employed various analytical methods to derive solutions for the wave equations (17-21). Simultaneously, numerical methods in this area have garnered significant interest from scientists (22-26).

Additionally, advancements in computational capabilities have enabled researchers to delve deeper into the complexities of wave dynamics, leading to a surge in interdisciplinary collaborations and the emergence of novel methodologies for wave analysis.

The numerical methods can be categorized into three distinct groups: macroscopic, microscopic, and mesoscopic. The latter, the mesoscopic methods, refer to a class of numerical techniques in the field of statistical mechanics that describe systems characterized by a large number of particles through probability strategies. Among these methods, the lattice Boltzmann method (LBM), known for its simplicity and efficiency (27), stands out as a strong tool that relies on the development of discrete particle distribution function at a mesoscopic level, on a lattice structure.

To date, numerous researchers have developed LBM to simulate various types of waves, including acoustic waves, surface acoustic waves, aeroacoustics waves, elastic waves, shock waves, electromagnetic waves, gravitational waves and, seismic waves (28-36). It can be said that the development of LBM for the simulation of wave propagation has been mainly done in two distinct approaches. The first is the direct solution of the Navier-Stokes equation based on instantaneous variables using the conventional LBM. Buick et al. (37) used the direct LBM to perform simulations of wave propagation in which the density fluctuation was relatively minor in comparison to the average density in the absence of the wave. Tan and Yeo (38) utilized a body force at the boundaries instead of implementing a density perturbation, to simulate wave propagation with the direct LBM. It is well known that this direct approach requires the creation of fine meshes and small time steps, which inevitably leads to higher computational costs and time. The second is solving the wave equations extracted from the Navier-Stokes equations based on acoustic variables, using LBM, which is a suitable alternative to overcome the limitations of the first approach. Chopard and Luthi (39) developed a new D2Q5 LB model with two relationships for the equilibrium distribution function to simulate wave propagation in complex geometries. Guangwu (40) performed simulations of 1D wave problems using a D1Q3 LB model and chose $\partial u(\boldsymbol{x},t)/\partial t$ as the zero-order macroscopic moment. This model has two relationships for the equilibrium distribution function and a truncation error of order 2. Zhang et al. (41, 42) presented a higher-order accuracy LB model for both D1Q5 and D2Q9 lattices to solve the wave equation. They used a Chapman–Enskog expansion for the distribution function up to the seventh order and obtained two new sets of five and nine independent relationships for the equilibrium distribution function. Lai and Ma (43) scrutinized LBM for generalized nonlinear 1D wave equations in a D1Q3 lattice, based on Guangwu's model (40). They obtained a new set of two independent relationships for the equilibrium distribution function. An and Bergada (44) numerically predicted the solution of mathematical–physical equations using a D2Q9 LB model. They adopted a third-degree polynomial for the equilibrium distribution function. By selecting some artificial complementary conditions, they presented an alternative collection of three independent relationships for the equilibrium distribution function to solve the 2D wave equation. Li et al. (45) proposed an LBGK model for simulating the damping wave equation, including the source term in (2+1)-dimensional wave with a D2Q9 scheme. They employed conservation conditions similar to those of Guangwu's model (40) and validated the algorithm with some exact solutions.

The reviewed papers in this section showed that many lattice Boltzmann (LB) models have been used to simulate wave propagation phenomena in various conditions. Among them, Table 1 displays various studies of the second approach in which lattice Boltzmann models have been used for the solution of different wave equations without damping terms. The table shows that two distinct choices of $u(\boldsymbol{x},t)$ or $\partial u(\boldsymbol{x},t)/\partial t$ are used for the zero-order macroscopic moment, resulting in 2 to 9 relationships for calculating the equilibrium distribution function. These relationships can only be used for one or two specific schemes of the

lattice Boltzmann method. It often poses a challenge in the application of these models for other lattice structures/schemes, since there is no single relationship for the equilibrium distribution function that can be used for different lattice structures.

So, it is valuable to seek a single relationship for the equilibrium distribution function (that is similar to the standard equilibrium distribution function). This study aims to obtain such a relationship by employing a generalized derivation method, which, to the best of the author's knowledge, has not yet been published in the LBM literature. Therefore, this paper focuses on this important issue by presenting a novel lattice-adaptive model that can simulate wave propagation with different initial and boundary conditions. The validity of the proposed model has been investigated using several test cases in 1D and 2D problems.

2. PROPOSED DERIVATION APPROACH

The governing equation of the LBM, which utilizes the Bhatnagar-Gross-Krook (BGK) approximation, is frequently denoted by the LBGK, where the particle distribution function, $f_i(\boldsymbol{x}, t)$, is used to simulate macroscopic fields. The distribution function's evolution equation in a standard LBGK method can be formulated through spatial and temporal discretization of the Boltzmann equation as:

$$f_i(\boldsymbol{x}+\boldsymbol{c}_i\Delta t, t+\Delta t) = f_i(\boldsymbol{x}, t) - \frac{1}{\tau}\left[f_i(\boldsymbol{x}, t) - f_i^{eq}(\boldsymbol{x}, t)\right] \quad (1)$$

where the lattice speed vector along a specific direction, i, is denoted by $\boldsymbol{c}_i$ and τ represents a single relaxation time parameter. It is worth mentioning that following the conservation laws, zero and first moments of the distribution function need to be equal to their corresponding equilibrium state, i.e., $\sum_i f_i = \sum_i f_i^{eq}$, $\sum_i \boldsymbol{c}_i f_i = \sum_i \boldsymbol{c}_i f_i^{eq}$ (46).

TABLE 1. Comparison of the models used for solving wave equations using LB

Different models	Lattice structure	Zero-order macroscopic moment*	# of Eqs. for f_i^{eq}	Ability to expand
[39], 1999	D2Q5	$u(\boldsymbol{x},t) = \sum_i f_i$	2	No
[40], 2000	D1Q3, D2Q5	$\frac{\partial u(\boldsymbol{x},t)}{\partial t} = \sum_i f_i$	2	No
[41], 2009	D1Q5	$u(\boldsymbol{x},t) = \sum_i f_i$	5	No
[42], 2009	D2Q9	$u(\boldsymbol{x},t) = \sum_i f_i$	9	No
[43], 2011	D1Q3	$\frac{\partial u(\boldsymbol{x},t)}{\partial t} = \sum_i f_i$	2	No
[44], 2016	D2Q9	$\frac{\partial u(\boldsymbol{x},t)}{\partial t} = \sum_i f_i$	3	No

* $u(\boldsymbol{x},t)$ is the displacement of the wave.

Within the proposed derivation approach, the equilibrium distribution function $f_i^{eq}(\boldsymbol{x}, t)$ of Equation 1 can be generally expressed as follows::

$$f_i^{eq} = \omega_i \phi_1 \left[A + B\frac{\boldsymbol{c}_i\cdot\boldsymbol{\phi}_2}{c_s^2} + D\frac{(\boldsymbol{c}_i\cdot\boldsymbol{\phi}_2)^2}{c_s^4} + E\frac{\boldsymbol{\phi}_2\cdot\boldsymbol{\phi}_2}{c_s^2}\right] \quad (2)$$

where coefficients A, B, D and E , as well as macroscopic variables ϕ_1 and $\boldsymbol{\phi_2}$, are unknowns that need to be determined according to the problem at hand. ω_i are weighting factors in direction i, whose values will be given later. Assuming unknown coefficients and then determining them is one of the features of this article. With such an approach, the equilibrium distribution function corresponding to the macroscopic equations of various problems can be independently determined with the help of Chapman-Enskog analysis.

It is worth mentioning that Equation 2 originates from Maxwell's distribution law, employing a second-order approximation through Taylor's expansion. The item c_s refers to the speed of sound in the lattice.

The discrete lattice speed vectors, $\boldsymbol{c}_i$, along the x, y directions and associated standard weighting factor ω_i for lattice structures D1Q3 (with i=0-2) and D2Q9 (with i=0-8), are defined by Equations 3a and 3b, respectively.

$$\begin{pmatrix} c_{ix} \\ \omega_i \end{pmatrix} = \begin{pmatrix} 0 & c & -c \\ \frac{2}{3} & \frac{1}{6} & \frac{1}{6} \end{pmatrix} \quad (3a)$$

$$\begin{pmatrix} c_{ix} \\ c_{iy} \\ \omega_i \end{pmatrix} = \begin{pmatrix} 0 & c & 0 & -c & 0 & c & -c & -c & c \\ 0 & 0 & c & 0 & -c & c & c & -c & -c \\ \frac{4}{9} & \frac{1}{9} & \frac{1}{9} & \frac{1}{9} & \frac{1}{9} & \frac{1}{36} & \frac{1}{36} & \frac{1}{36} & \frac{1}{36} \end{pmatrix} \quad (3b)$$

where $c = \Delta x/\Delta t = \Delta y/\Delta t$ stands for lattice speed, Δx and Δy are space steps and also Δt is the time step. The schematic representation of lattice structures D1Q3 and D2Q9 can be seen in Figure 1.

The weighting factor ω_i also satisfies the requirements listed in Equation 4 (46).

$$\begin{cases} \sum_i \omega_i = 1, & \sum_i \boldsymbol{c}_i\omega_i = 0 \\ \sum_i \boldsymbol{c}_i\boldsymbol{c}_i\omega_i = c_s^2\,\boldsymbol{I}, & \sum_i \boldsymbol{c}_i\boldsymbol{c}_i\boldsymbol{c}_i\omega_i = 0 \\ \sum_i \boldsymbol{c}_i\boldsymbol{c}_i\boldsymbol{c}_i\boldsymbol{c}_i\omega_i = 3c_s^4\boldsymbol{II}, & \sum_i \boldsymbol{c}_i\boldsymbol{c}_i\boldsymbol{c}_i\boldsymbol{c}_i\boldsymbol{c}_i\omega_i = 0 \end{cases} \quad (4)$$

To succeed in recovering the desired macroscopic equation from the lattice Boltzmann equation, f_i^{eq} must

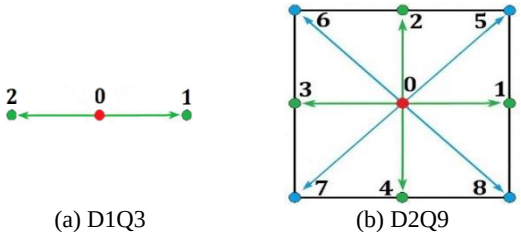

(a) D1Q3 (b) D2Q9

Figure 1. Schematic representation of the lattice structures D1Q3 and D2Q9 (D: Dimension, Q: Velocities on the discrete lattice)

satisfy the equilibrium moments as follows (46). It is important to note that the unknown coefficients in Equation 2, namely, A, B, D and E, and also ϕ_1 and $\boldsymbol{\phi_2}$ are depend on the physical problem.

For example, employing Taylor expansion and Chapman-Enskog analysis, one can show that for an incompressible fluid flow problem, Equation 2 will reduce to a familiar form as follows (47-49):

$$f_i^{eq} = \omega_i \rho \left[1 + \frac{\boldsymbol{c}_i \cdot \boldsymbol{v}}{{c_s}^2} + \frac{1}{2}\left(\frac{\boldsymbol{c}_i \cdot \boldsymbol{v}}{{c_s}^2}\right)^2 - \frac{1}{2}\frac{\boldsymbol{v} \cdot \boldsymbol{v}}{{c_s}^2}\right] \tag{5}$$

while the macroscopic variables need to be chosen as follows:

$$\rho = \sum_i f_i \,,\ \rho \boldsymbol{v} = \sum_i \boldsymbol{c}_i f_i \,,\ \rho c_s^2 \boldsymbol{I} + \rho \boldsymbol{v}\boldsymbol{v} = \sum_i \boldsymbol{c}_i \boldsymbol{c}_i f_i^{eq} \tag{6}$$

where ρ and $\boldsymbol{v}$ are the macroscopic density and velocity vector of the flow problem. It is worth mentioning that Equation 5 is called the standard equilibrium distribution function, and ω_i is its standard weighting factor for different lattice structures in LBM.

2. 1. Exerting the Proposed Approach for the Wave Equation The approach introduced in this paper, based on Equation 2, is carried out to find the equilibrium distribution function so that the wave equation can be recovered. The traditional way is to apply Taylor expansion and Chapman-Enskog analysis to determine the equilibrium distribution function and its moments for a physical problem so that the LBGK equation (Equation 1) can correspond to it. The linear wave equation in operator form is given as follows:

$$\frac{\partial^2 u}{\partial t^2} = c_s^2 \nabla^2 u \tag{7}$$

where $u = u(\boldsymbol{x},t)$ is the displacement of the wave and ∇^2 is the Laplacian operator. In this paper, u as a general variable, represents the displacement of the acoustic pressure (p') or acoustic density (ρ') in Equation 7 as the "linear acoustic wave equation".

The Chapman-Enskog analysis is utilized for expanding the distribution function, temporal derivatives, and spatial derivatives around their equilibrium values, as follows (44):

$$\begin{cases} f_i = f_i^{(0)} + \varepsilon f_i^{(1)} + \varepsilon^2 f_i^{(2)} \\ \frac{\partial}{\partial t} = \varepsilon \frac{\partial}{\partial t_1} + \varepsilon^2 \frac{\partial}{\partial t_2} \\ \boldsymbol{\nabla} = \varepsilon \boldsymbol{\nabla_1} \end{cases} \tag{8}$$

where the dimensionless variable ε is viewed as a small parameter. Moreover, $f_i^{(1)}$ and $f_i^{(2)}$ in Equation 8, satisfy the conservation laws as follows (46):

$$\begin{cases} \sum_i f_i^{(1)} = \sum_i f_i^{(2)} = 0 \\ \sum_i \boldsymbol{c}_i f_i^{(1)} = \sum_i \boldsymbol{c}_i f_i^{(2)} = 0 \end{cases} \tag{9}$$

Moreover, for simplicity, one can use the following definition for the macroscopic variables.

$$\Pi_0^{eq} = \sum_i f_i^{eq} \,,\ \boldsymbol{\Pi_1^{eq}} = \sum_i \boldsymbol{c}_i f_i^{eq} \,,\ \boldsymbol{\Pi_2^{eq}} = \sum_i \boldsymbol{c}_i \boldsymbol{c}_i f_i^{eq} \tag{10}$$

where, f_i^{eq}, must be determined based on the problem at hand, say wave problem. Employing the two-variable Taylor expansion of f_i at a given point $(\boldsymbol{x}, t)$, one can derive the result as follows:

$$\begin{aligned} f_i(\boldsymbol{x} + \boldsymbol{c}_i \Delta t, t + \Delta t) &= f_i(\boldsymbol{x}, t) + \Delta t \left(\frac{\partial}{\partial t} + \boldsymbol{c}_i \cdot \boldsymbol{\nabla}\right) f_i \\ &+ \frac{\Delta t^2}{2}\left(\frac{\partial}{\partial t} + \boldsymbol{c}_i \cdot \boldsymbol{\nabla}\right)^2 f_i \end{aligned} \tag{11}$$

Introducing Equations 11 and 8 into Equation 1 results in:

$$\begin{aligned} &\left(\varepsilon \frac{\partial}{\partial t_1} + \varepsilon^2 \frac{\partial}{\partial t_2} + \varepsilon\, \boldsymbol{c}_i \cdot \boldsymbol{\nabla_1}\right)\left(f_i^{(0)} + \varepsilon f_i^{(1)} + \varepsilon^2 f_i^{(2)}\right) \\ &+ \frac{\Delta t}{2}\left(\varepsilon \frac{\partial}{\partial t_1} + \varepsilon^2 \frac{\partial}{\partial t_2} + \varepsilon\, \boldsymbol{c}_i \cdot \boldsymbol{\nabla_1}\right)^2 \left(f_i^{(0)} + \varepsilon f_i^{(1)} + \varepsilon^2 f_i^{(2)}\right) \\ &= \frac{-1}{\tau \Delta t}\left[f_i^{(0)} + \varepsilon f_i^{(1)} + \varepsilon^2 f_i^{(2)} - f_i^{eq}\right] \end{aligned} \tag{12}$$

By equating order by order and keeping terms only up to $\mathcal{O}(\varepsilon^2)$, one can obtain the following set of equations:

$$\varepsilon^0: \quad f_i^{(0)} = f_i^{eq} \tag{13a}$$

$$\varepsilon^1: \quad \left(\frac{\partial}{\partial t_1} + \boldsymbol{c}_i \cdot \boldsymbol{\nabla_1}\right) f_i^{(0)} = -\frac{1}{\tau \Delta t} f_i^{(1)} \tag{13b}$$

$$\begin{aligned} \varepsilon^2: &\left(\frac{\partial}{\partial t_1} + \boldsymbol{c}_i \cdot \boldsymbol{\nabla_1}\right) f_i^{(1)} + \frac{\Delta t}{2}\left(\frac{\partial}{\partial t_1} + \boldsymbol{c}_i \cdot \boldsymbol{\nabla_1}\right)^2 f_i^{(0)} \\ &+ \frac{\partial f_i^{(0)}}{\partial t_2} = -\frac{1}{\tau \Delta t} f_i^{(2)} \end{aligned} \tag{13c}$$

Substituting Equation 13b into Equation 13c and rearranging gives:

$$\Delta t\left(\frac{1}{2} - \tau\right)\left(\frac{\partial}{\partial t_1} + \boldsymbol{c}_i \cdot \boldsymbol{\nabla_1}\right)^2 f_i^{(0)} + \frac{\partial f_i^{(0)}}{\partial t_2} = -\frac{1}{\tau \Delta t} f_i^{(2)} \tag{14}$$

Summing Equation 13b over the whole set of discrete directions *i*, and with the help of Equations 9 and 10, it is obtained as:

$$\frac{\partial}{\partial t_1} \Pi_0^{eq} + \boldsymbol{\nabla_1} \cdot \boldsymbol{\Pi_1^{eq}} = 0 \tag{15}$$

Multiplying Equation 14 by $\boldsymbol{c}_i$ before summing over i, and then calculating the divergence of the resulting equation gives:

$$\frac{\partial}{\partial t_1}\left(\boldsymbol{\nabla_1} \cdot \boldsymbol{\Pi_1^{eq}}\right) + \boldsymbol{\nabla_1} \cdot \left(\boldsymbol{\nabla_1} \cdot \boldsymbol{\Pi_2^{eq}}\right) = 0 \tag{16}$$

Summing Equation 13c over the whole set of discrete directions *i*, and with the help of Equations 9 and 10, it is obtained as:

$$\begin{aligned} \frac{\partial}{\partial t_2} \Pi_0^{eq} &= -\frac{\Delta t}{2} \frac{\partial^2}{\partial t_1^2} \Pi_0^{eq} - \Delta t \frac{\partial}{\partial t_1}\left(\boldsymbol{\nabla_1} \cdot \boldsymbol{\Pi_1^{eq}}\right) \\ &- \frac{\Delta t}{2} \boldsymbol{\nabla_1} \cdot \left(\boldsymbol{\nabla_1} \cdot \boldsymbol{\Pi_2^{eq}}\right) \end{aligned} \tag{17}$$

By taking the temporal derivative $(\partial / \partial t_1)$ of Equation 15, substituting it into the right-hand side of Equation 17, and with the help of Equation 16, one can obtain as:

$$\frac{\partial}{\partial t_2}\Pi_0^{eq}=0 \tag{18}$$

Constructing the subsequent operation $\varepsilon\times$Equation (15) + $\varepsilon^2\times$ Equation 18, it is acquired as:

$$\frac{\partial}{\partial t}\Pi_0^{eq}+\boldsymbol{\nabla}\cdot\boldsymbol{\Pi_1^{eq}}=0 \tag{19}$$

Constructing the subsequent operation $(\varepsilon\boldsymbol{c}_i)$.(Equation (13b)) $+(\varepsilon^2\boldsymbol{c}_i)$.(Equation 14 + Equation 18), and then summing over i, it is obtained as:

$$\begin{aligned}&\varepsilon\frac{\partial}{\partial t_1}\textstyle\sum_i \boldsymbol{c}_i f_i^{(0)}+\varepsilon^2\frac{\partial}{\partial t_2}\sum_i \boldsymbol{c}_i f_i^{(0)}+\varepsilon\boldsymbol{\nabla}_1\cdot\sum_i \boldsymbol{c}_i\boldsymbol{c}_i f_i^{(0)}\\&+\varepsilon^2\Delta t\left(\tfrac{1}{2}-\tau\right)\sum_i \boldsymbol{c}_i\left(\frac{\partial}{\partial t_1}+\boldsymbol{c}_i\cdot\boldsymbol{\nabla}_1\right)^2 f_i^{(0)}\\&=-\tfrac{1}{\tau\Delta t}\textstyle\sum_i\left(\varepsilon\boldsymbol{c}_i f_i^{(1)}+\varepsilon^2\boldsymbol{c}_i f_i^{(2)}\right)\end{aligned} \tag{20}$$

It is obvious that by using Equation 9, the right-hand side of Equation 20 equates to zero. In addition, using Equations 9 and 10, the simplified form for the summation of the first two terms on the left-hand side of Equation 20 is obtained as:

$$\varepsilon\frac{\partial}{\partial t_1}\textstyle\sum_i \boldsymbol{c}_i f_i^{(0)}+\varepsilon^2\frac{\partial}{\partial t_2}\sum_i \boldsymbol{c}_i f_i^{(0)}=\frac{\partial}{\partial t}\boldsymbol{\Pi_1^{eq}} \tag{21}$$

with the help of the conditions in Equation 4 and Equation 2, the third term on the left-hand side of Equation 20 becomes:

$$\begin{aligned}&\varepsilon\boldsymbol{\nabla}_1\cdot\textstyle\sum_i \boldsymbol{c}_i\boldsymbol{c}_i f_i^{(0)}=\boldsymbol{\nabla}\cdot\Big(A\phi_1\sum_i \boldsymbol{c}_i\boldsymbol{c}_i\omega_i+\\&D\tfrac{\phi_1\boldsymbol{\phi}_2\cdot\boldsymbol{\phi}_2}{c_s^4}\sum_i \boldsymbol{c}_i\boldsymbol{c}_i\boldsymbol{c}_i\boldsymbol{c}_i\omega_i+E\tfrac{\phi_1\boldsymbol{\phi}_2\cdot\boldsymbol{\phi}_2}{c_s^2}\sum_i \boldsymbol{c}_i\boldsymbol{c}_i\omega_i\Big)\end{aligned} \tag{22}$$

The expanded form of the fourth term on the left-hand side of Equation 20 gives:

$$\begin{aligned}&\varepsilon^2\Delta t\left(\tfrac{1}{2}-\tau\right)\textstyle\sum_i \boldsymbol{c}_i\left(\frac{\partial}{\partial t_1}+\boldsymbol{c}_i\cdot\boldsymbol{\nabla}_1\right)^2 f_i^{(0)}\\&=\varepsilon^2\Delta t\left(\tfrac{1}{2}-\tau\right)\textstyle\sum_i \boldsymbol{c}_i(\boldsymbol{c}_i\cdot\boldsymbol{\nabla_1})^2 f_i^{(0)}\\&+\varepsilon^2\Delta t\left(\tfrac{1}{2}-\tau\right)\frac{\partial}{\partial t_1}\sum_i \boldsymbol{c}_i\left(\frac{\partial}{\partial t_1}+2\boldsymbol{c}_i\cdot\boldsymbol{\nabla}_1\right)f_i^{(0)}\end{aligned} \tag{23}$$

Applying Equations 4 and 2 in the first term on the right-hand side of Equation 23, give:

$$\begin{aligned}&\varepsilon^2\Delta t\left(\tfrac{1}{2}-\tau\right)\textstyle\sum_i \boldsymbol{c}_i(\boldsymbol{c}_i\cdot\boldsymbol{\nabla_1})^2 f_i^{(0)}\\&=\Delta t\left(\tfrac{1}{2}-\tau\right)\boldsymbol{\nabla}\cdot\Big(\boldsymbol{\nabla}\cdot\big(B\tfrac{\phi_1\boldsymbol{\phi}_2}{c_s^2}\cdot\textstyle\sum_i \boldsymbol{c}_i\boldsymbol{c}_i\boldsymbol{c}_i\boldsymbol{c}_i\omega_i\big)\Big)\end{aligned} \tag{24}$$

By summing Equation 13b over i, taking the temporal derivative $(\partial/\partial t_1)$ of this equation, and then multiplying the resulting expression by $\left(-\varepsilon^2\boldsymbol{c}_i\Delta t\left(\frac{1}{2}-\tau\right)\right)$, one can obtain:

$$-\varepsilon^2\Delta t\left(\tfrac{1}{2}-\tau\right)\frac{\partial}{\partial t_1}\left(\textstyle\sum_i \boldsymbol{c}_i\left(\frac{\partial}{\partial t_1}+\boldsymbol{c}_i\cdot\nabla_1\right)f_i^{(0)}\right)=0 \tag{25}$$

Adding Equation 25 to the second term on the right-hand side of Equation 23 yields:

$$\begin{aligned}&\varepsilon^2\Delta t\left(\tfrac{1}{2}-\tau\right)\frac{\partial}{\partial t_1}\textstyle\sum_i \boldsymbol{c}_i\left(\frac{\partial}{\partial t_1}+2\boldsymbol{c}_i\cdot\nabla_1\right)f_i^{(0)}-\varepsilon^2\Delta t\left(\tfrac{1}{2}-\right.\\&\left.\tau\right)\frac{\partial}{\partial t_1}\left(\textstyle\sum_i \boldsymbol{c}_i\left(\frac{\partial}{\partial t_1}+\boldsymbol{c}_i\cdot\nabla_1\right)f_i^{(0)}\right)=\varepsilon^2\Delta t\left(\tfrac{1}{2}-\right.\\&\left.\tau\right)\frac{\partial}{\partial t_1}\textstyle\sum_i \boldsymbol{c}_i(\boldsymbol{c}_i\cdot\nabla_1)f_i^{(0)}\end{aligned} \tag{26}$$

Substituting Equation 2 into Equation 26, using Equation 4 and rearranging, give:

$$\begin{aligned}&\varepsilon^2\Delta t\left(\tfrac{1}{2}-\tau\right)\frac{\partial}{\partial t_1}\textstyle\sum_i \boldsymbol{c}_i(\boldsymbol{c}_i\cdot\nabla_1)f_i^{(0)}=\varepsilon\Delta t\left(\tfrac{1}{2}-\tau\right)\\&\frac{\partial}{\partial t_1}\boldsymbol{\nabla}\cdot\Big(A\phi_1\textstyle\sum_i \boldsymbol{c}_i\boldsymbol{c}_i\omega_i+D\frac{\phi_1\boldsymbol{\phi}_2\cdot\boldsymbol{\phi}_2}{c_s^4}\sum_i \boldsymbol{c}_i\boldsymbol{c}_i\boldsymbol{c}_i\boldsymbol{c}_i\omega_i+\\&E\tfrac{\phi_1\boldsymbol{\phi}_2\cdot\boldsymbol{\phi}_2}{c_s^2}\textstyle\sum_i \boldsymbol{c}_i\boldsymbol{c}_i\omega_i\Big)\end{aligned} \tag{27}$$

where $B\sum_i \boldsymbol{c}_i\boldsymbol{c}_i\boldsymbol{c}_i\omega_i=0$. Substituting Equations 21, 22, 24, and 27 into Equation 20 and choosing $\tau=1/2$ (44) results in:

$$\begin{aligned}&\frac{\partial}{\partial t}\boldsymbol{\Pi_1^{eq}}+\boldsymbol{\nabla}\cdot\Big(A\phi_1\textstyle\sum_i \boldsymbol{c}_i\boldsymbol{c}_i\omega_i+D\frac{\phi_1\boldsymbol{\phi}_2\cdot\boldsymbol{\phi}_2}{c_s^4}\sum_i \boldsymbol{c}_i\boldsymbol{c}_i\boldsymbol{c}_i\boldsymbol{c}_i\omega_i+\\&E\tfrac{\phi_1\boldsymbol{\phi}_2\cdot\boldsymbol{\phi}_2}{c_s^2}\textstyle\sum_i \boldsymbol{c}_i\boldsymbol{c}_i\omega_i\Big)=0\end{aligned} \tag{28}$$

It is important to emphasize that the selection of relaxation time equal to $1/2$ in Equation 28 implies neglecting viscous dissipation.

Taking $\boldsymbol{\nabla}\cdot$ (Equation 28) $-\frac{\partial}{\partial t}$ (Equation 19), gives:

$$\begin{aligned}&\frac{\partial}{\partial t}\left(\boldsymbol{\nabla}\cdot\boldsymbol{\Pi_1^{eq}}\right)+\boldsymbol{\nabla}\cdot\Big(\boldsymbol{\nabla}\cdot\big(A\phi_1\textstyle\sum_i \boldsymbol{c}_i\boldsymbol{c}_i\omega_i+\\&D\tfrac{\phi_1\boldsymbol{\phi}_2\cdot\boldsymbol{\phi}_2}{c_s^4}\sum_i \boldsymbol{c}_i\boldsymbol{c}_i\boldsymbol{c}_i\boldsymbol{c}_i\omega_i+E\tfrac{\phi_1\boldsymbol{\phi}_2\cdot\boldsymbol{\phi}_2}{c_s^2}\textstyle\sum_i \boldsymbol{c}_i\boldsymbol{c}_i\omega_i\big)\Big)\\&-\frac{\partial}{\partial t}\left(\frac{\partial}{\partial t}\Pi_0^{eq}\right)-\frac{\partial}{\partial t}\left(\boldsymbol{\nabla}\cdot\boldsymbol{\Pi_1^{eq}}\right)=0\end{aligned} \tag{29}$$

Equation 29 can be summarized as:

$$\begin{aligned}&\frac{\partial^2}{\partial t^2}\Pi_0^{eq}=\boldsymbol{\nabla}\cdot\Big(\boldsymbol{\nabla}\cdot\big(A\phi_1\textstyle\sum_i \boldsymbol{c}_i\boldsymbol{c}_i\omega_i+\\&D\tfrac{\phi_1\boldsymbol{\phi}_2\cdot\boldsymbol{\phi}_2}{c_s^4}\sum_i \boldsymbol{c}_i\boldsymbol{c}_i\boldsymbol{c}_i\boldsymbol{c}_i\omega_i+E\tfrac{\phi_1\boldsymbol{\phi}_2\cdot\boldsymbol{\phi}_2}{c_s^2}\textstyle\sum_i \boldsymbol{c}_i\boldsymbol{c}_i\omega_i\big)\Big)\end{aligned} \tag{30}$$

The macroscopic wave equation (Equation 7) can be generated by substituting Equation 4 into Equation 30 by just letting:

$$\begin{cases}A\phi_1=\Pi_0^{eq}=u\\D=E=0\end{cases} \tag{31}$$

It is worth mentioning that one could set $D=E=0$ in Equation 2 because the problem at hand is a linear case, however, to preserve the generality of the process, this setting is postponed to Equation 31.

To calculate the remaining unknown coefficient B and function $\boldsymbol{\phi_2}$, it is possible to substitute Equation 2 into Equation 10, and use Equation 4, which gives:

$$B\boldsymbol{\phi_2}=\frac{\boldsymbol{\Pi_1^{eq}}}{\left(\frac{\Pi_0^{eq}}{A}\right)} \tag{32}$$

and finally, the f_i^{eq} is determined using a simple equation as follows:

$$f_i^{eq}=\omega_i\left[u+\tfrac{\boldsymbol{c}_i\cdot\boldsymbol{\Pi_1^{eq}}}{c_s^2}\right] \tag{33}$$

where $u = \sum_i f_i$ is the zero-order macroscopic moment, $\boldsymbol{\Pi}_{\mathbf{1}}^{\boldsymbol{eq}} = \sum_{\boldsymbol{i}} \boldsymbol{c}_i f_i = \sum_i \boldsymbol{c}_i f_i^{eq}$ is the first-order macroscopic moment, and ω_i is the standard weighting factor (Equation 3).

Therefore, as expected, a new single relationship is obtained for the equilibrium distribution function, which can be easily used for simulating linear wave equations in different lattice structures based on Table 2. Another important aspect concerning Equation 33 is that this equation uses $u(\boldsymbol{x},t)$ as a zero-order macroscopic moment, unlike many common models employing $\partial u(\boldsymbol{x},t)/\partial t$, to solve the wave equation, which is comparable to the usual form of the lattice Boltzmann.

2. 2. Error Calculation Formulas The four different error norms are used to assess the precision of the current model. These error norms include the relative error norm E_2 defined by Equation 34, the maximum error norm E_∞ defined by Equation 35, the global relative error norm GRE defined by Equation 36, and the root mean square error norm RMS defined by Equation 37 as follows:

$$E_2 = \left(\sum_{i=1}^{Nx}\sum_{j=1}^{Ny}|u(x_i,y_j,t) - u^*(x_i,y_j,t)|^2 / \sum_{i=1}^{Nx}\sum_{j=1}^{Ny}|u^*(x_i,y_j,t)|^2\right)^{\frac{1}{2}} \quad (34)$$

$$E_\infty = max|u(x_i,y_j,t) - u^*(x_i,y_j,t)| \quad i = 1,2,\ldots,Nx \quad j = 1,2,\ldots,Ny \quad (35)$$

$$GRE = \left(\sum_{i=1}^{Nx}\sum_{j=1}^{Ny}|u(x_i,y_j,t) - u^*(x_i,y_j,t)| / \sum_{i=1}^{Nx}\sum_{j=1}^{Ny}|u^*(x_i,y_j,t)|\right) \quad (36)$$

$$RMS = \left(\sum_{i=1}^{Nx}\sum_{j=1}^{Ny}|u(x_i,y_j,t) - u^*(x_i,y_j,t)|^2 / (N_x \times N_y)\right)^{\frac{1}{2}} \quad (37)$$

Among these $u(x_i,y_j,t)$ and $u^*(x_i,y_j,t)$ are numerical and analytical results, respectively. The information from all mesh points is summed to calculate the summation terms.

3. VALIDATION ON 1D WAVE EQUATION

In this section, three benchmark test cases are validated to verify the accuracy and efficiency of the proposed model for the 1D wave equation:

$$\frac{\partial^2 u}{\partial t^2} = c_s^2 \frac{\partial^2 u}{\partial x^2}, \quad 0 \le x \le 1, \quad 0 < t \quad (38)$$

The numerical results are compared with exact solutions for all test cases, including different initial and boundary conditions.

3. 1. Sin-shaped Initial Condition (Test Case 1) The focus of this benchmark test case is to examine the 1D wave equation (Equation 38) with sinusoidal initial conditions as:

$$\begin{cases} u(x,0) = A\ sin(\pi x) \\ u_t(x,0) = 0 \end{cases} \quad (39)$$

The boundary conditions are:

$$\begin{cases} u(0,t) = 0 \\ u(1,t) = 0 \end{cases} \quad (40)$$

The analytical solution for this case can be found in literature (50):

$$u(x,t) = A\ sin(\pi x)\ cos(\pi c_s t) \quad (41)$$

where A represents the amplitude of the wave. In what follows, it is taken $\Delta x = 1 \times 10^{-3}$, $\Delta t = 1 \times 10^{-4}$, $c_s = 5.77$, and $c = 10.0$

Figure 2 illustrates the comparison between a 3-bit 1D numerical prediction of the present model (D1Q3) with an analytical solution extracted from Equation 41 for $u(x,t)$ up to t= 3.2 s. Although this figure shows good agreement, it just provides an overview of the comparison. Thus, a 2D view analysis of the performance of the model is necessary to better understand its accuracy which this view is shown in Figure 3. The numerical solutions are represented by discrete symbols, and the analytical solutions are represented by solid lines in Figure 3. It shows that the outcomes from two models are nearly equivalent at different instant times, t=0.8 s,

TABLE 2. Comparison between the present lattice adaptive model based on the new equilibrium distribution function (Equation 33) and other models for solving linear acoustic wave equations

Different models	Lattice structure								# of equations
	D1Q2	D1Q3	D2Q4	D2Q5	D2Q9	D3Q15	D3Q19	D3Q27	
This work	✓	✓	✓	✓	✓	✓	✓	✓	1
[39], 1999	✓	✓	✓	✓	×	×	×	×	2
[40], 2000	✓	✓	✓	✓	×	×	×	×	2
[41], 2009	×	✓	×	×	×	×	×	×	5
[42], 2009	×	×	×	×	✓	×	×	×	9
[43], 2011	✓	✓	×	×	×	×	×	×	2
[44], 2016	×	×	×	×	✓	×	×	×	3

t=1.6 s, t=2.4 s, and t=3.2 s. Take note that the agreement is great. Moreover, the numerical solution accurately captures the characteristics of wave motion. A standing wave is forming, with two nodes at the fixed ends and one antinode in the middle. The wavelength remains constant; however, the wave's displacement exhibits an oscillatory motion: rising from an initial value to its maximum value and then falling back to its initial value. Also, in the present test case, the errors of $u(x,t)$ are calculated and listed in Table 3. The table shows different standard errors, including E_2, E_∞, GRE, and RMS at particular times, namely, t=0.8 s, t=1.6 s, t=2.4 s, and t=3.2 s.

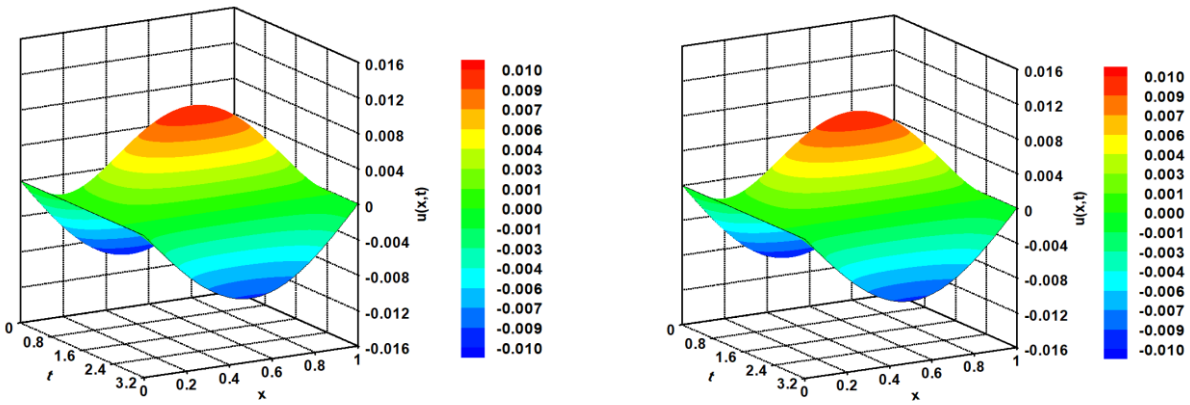

(a) (b)

Figure 2. Space-time evolution graph of the numerical results (a) and analytical results (b) for $u(x,t)$ from t=0 to t = 3.2 s for test case 1

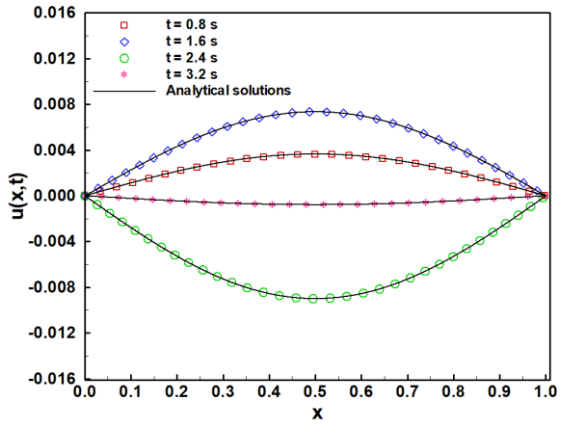

Figure 3. Comparison between numerical simulations (symbols) and analytical solutions (solid lines) for $u(x,t)$ at various times for test case 1

The relative error norm E_2 is displayed in Figure 4 at different lattice spacing where numerical simulations have been fixed at t = 1.0 s. In this figure, the slopes of the fitting line are extremely close to 2 (1.964), which indicates that the current model possesses a spatial accuracy of second-order. In addition, as the mesh size becomes more refined, a decrease in errors is noticeable.

3. 2. Pulse-shaped Initial Condition (Test Case 2)

The focus of this benchmark test case is to examine the 1D wave equation (Equation 38) with pulse/bell-shaped initial conditions as follows:

$$\begin{cases} u(x,0) = \frac{0.2}{1+9x^2} \\ u_t(x,0) = 0 \end{cases} \quad (42)$$

The boundary conditions are:

TABLE 3. The comparison of error norms E_2, E_∞, GRE, and RMS for $u(x,t)$ at various times for test case 1

t (s)	Error norms			
	E_2	E_∞	GRE	RMS
0.8	4.6438×10^{-3}	1.6932×10^{-5}	4.6438×10^{-3}	1.1967×10^{-5}
1.6	1.6835×10^{-3}	1.2358×10^{-5}	1.6835×10^{-3}	8.7343×10^{-6}
2.4	8.8610×10^{-4}	7.9746×10^{-6}	8.8610×10^{-4}	5.6361×10^{-6}
3.2	6.0966×10^{-4}	5.7854×10^{-6}	6.0966×10^{-4}	4.0888×10^{-6}

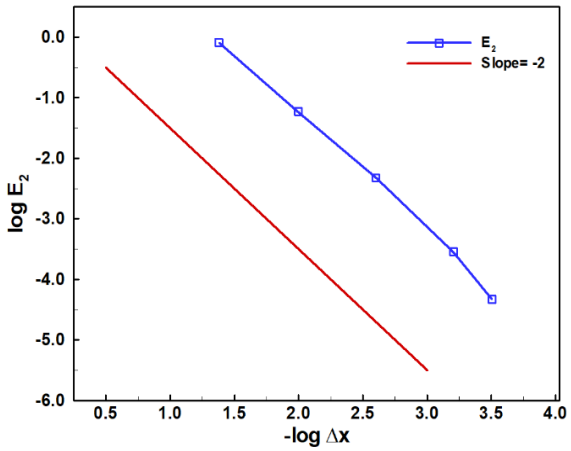

Figure 4. The accuracy test of the relative error norm (E_2) at various lattice sizes for test case 1. The slope of the red line is equal to -2

$$\begin{cases} u(0,t) = \frac{0.1}{1+9(5+c_s t)^2} + \frac{0.1}{1+9(-5+c_s t)^2} \\ u(1,t) = \frac{0.1}{1+9(5-c_s t)^2} + \frac{0.1}{1+9(5+c_s t)^2} \end{cases} \quad (43)$$

The analytical solution for this case can be found in literature [40] as:

$$u(x,t) = \frac{0.1}{1+9(10x-5-c_s t)^2} + \frac{0.1}{1+9(10x-5+c_s t)^2} \quad (44)$$

In this proceeding, it is adopted $\Delta x = 1 \times 10^{-3}$, $\Delta t = 5 \times 10^{-4}$, $c_s = 1.15$, and $c = 2.0$.

Figure 5 compares a 3-bit 1D scheme (D1Q3) of the present model to an analytical solution extracted from Equation 44 for $u(x,t)$ up to 3.2 s. For a clearer evaluation of the model accuracy at different times, Figure 6 provides a 2D view of the comparison of numerical solutions (discrete symbols) and analytical solutions (solid lines). As shown in Figures 5 and 6, the

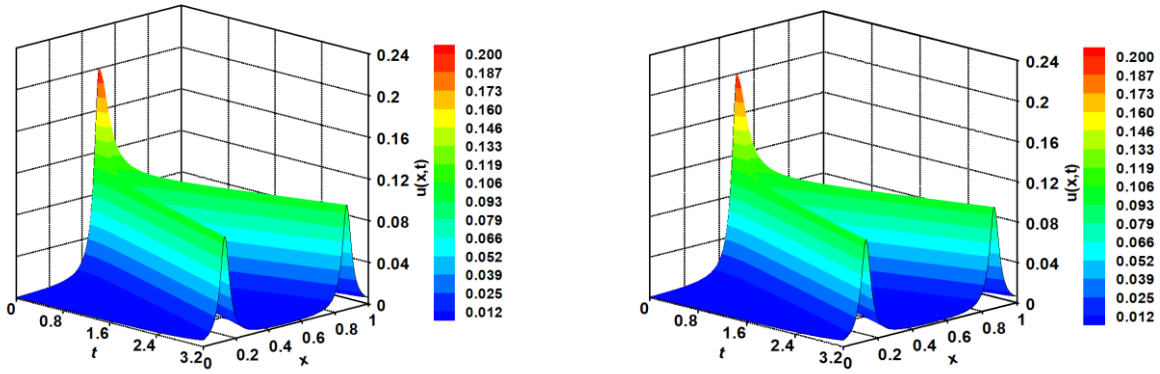

(a) (b)

Figure 5. Space-time evolution graph of the numerical results (a) and analytical results (b) for $u(x,t)$ from t=0 to t = 3.2 s for test case 2

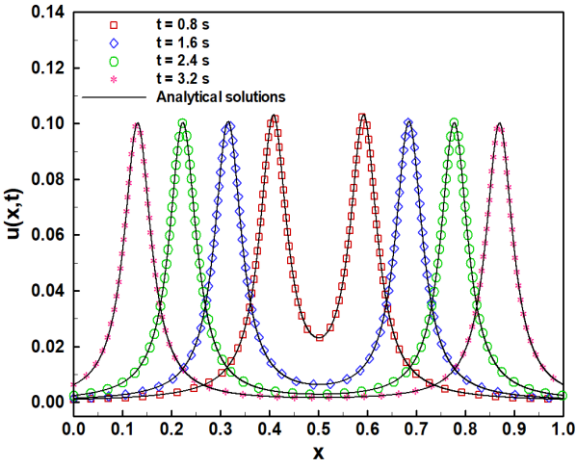

Figure 6. Comparison between numerical simulations (symbols) and analytical solutions (solid lines) for $u(x,t)$ at various times for test case 2

numerical solutions have good agreement with the corresponding analytical solutions at different instant times t=0.8 s, t=1.6 s, t=2.4 s, and t=3.2 s. The wave has an initial displacement comparable to a Gaussian distribution and then splits into two left- and right-traveling wave packets. The wave's amplitude rapidly decreases up to roughly t=1 s before remaining constant throughout. Also, in the present test case, the errors of $u(x,t)$ are calculated and listed in Table 4. The table shows different standard errors, including E_2, E_∞, GRE, and RMS at particular times, namely, t=0.8 s, t=1.6 s, t=2.4 s, and t=3.2 s.

3. 3. Zero Initial Condition (Test Case 3) The focus of this benchmark test case is to investigate the 1D wave equation (Equation 38) with zero initial conditions and a constant boundary feed provided by the non-zero Newman boundary condition as follows:

$$\begin{cases} u(x,0) = 0 \\ u_t(x,0) = 0 \end{cases} \quad (45)$$

$$\begin{cases} u(0,t) = 0 \\ u_x(1,t) = g_0 \end{cases} \quad (46)$$

The analytical solution for this equation can be found in literature (40) as:

$$u(x,t) = C_s\, g_0 \left[\left(t - \frac{1-x}{c_s}\right) \mathcal{H}\left(t - \frac{1-x}{c_s}\right) - \left(t - \frac{1+x}{c_s}\right) \mathcal{H}\left(t - \frac{1+x}{c_s}\right) - \left(t - \frac{3-x}{c_s}\right) \mathcal{H}\left(t - \frac{3-x}{c_s}\right) + \left(t - \frac{3+x}{c_s}\right) \mathcal{H}\left(t - \frac{3+x}{c_s}\right)\right] \quad (47)$$

where $\mathcal{H}(\xi)$ represents the Heaviside function. In what follows, it is taken $\Delta x = 1 \times 10^{-3}$, $\Delta t = 1 \times 10^{-3}$, $c_s = 0.577$, $c = 1.0$, $0 < t < \frac{4}{c_s}$, and $g_0 = 0.1$.

Figure 7 illustrates the comparison between a 3-bit 1D scheme (D1Q3) of the present model and an analytical solution extracted from Equation 47 for u(x,t) up to t= 1.6 s. For a clearer evaluation of the model accuracy at different times, Figure 8 provides a 2D view of the comparison of numerical solutions (discrete symbols) and analytical solutions (solid lines). As illustrated in Figures 7 and 8, the numerical solutions show good agreement with the corresponding analytical solutions at different instant times t=0.4 s, t=0.8 s, t=1.2 s, and t=1.6 s. Moreover, the motion properties of the wave propagation are well reflected by the numerical solution: the amplitude of the wave at the right boundary increases with time to keep u_x constant. Additionally, in the present test case, the errors of $u(x,t)$ are calculated and listed in Table 5. The table shows different standard errors, including E_2, E_∞, GRE, and RMS at particular times, namely, t=0.4 s, t=0.8 s, t=1.2 s, and t=1.6 s.

TABLE 4. Comparison of error norms E_2, E_∞, GRE, and RMS for $u(x,t)$ at various times for test case 2

t (s)	Error norms			
	E_2	E_∞	GRE	RMS
0.8	1.1807×10^{-3}	1.1532×10^{-4}	1.1153×10^{-3}	4.0341×10^{-5}
1.6	1.2107×10^{-3}	1.1320×10^{-4}	1.1443×10^{-3}	3.9782×10^{-5}
2.4	1.2203×10^{-3}	1.1324×10^{-4}	1.1526×10^{-3}	3.9751×10^{-5}
3.2	1.2216×10^{-3}	1.1388×10^{-4}	1.1578×10^{-3}	3.9618×10^{-5}

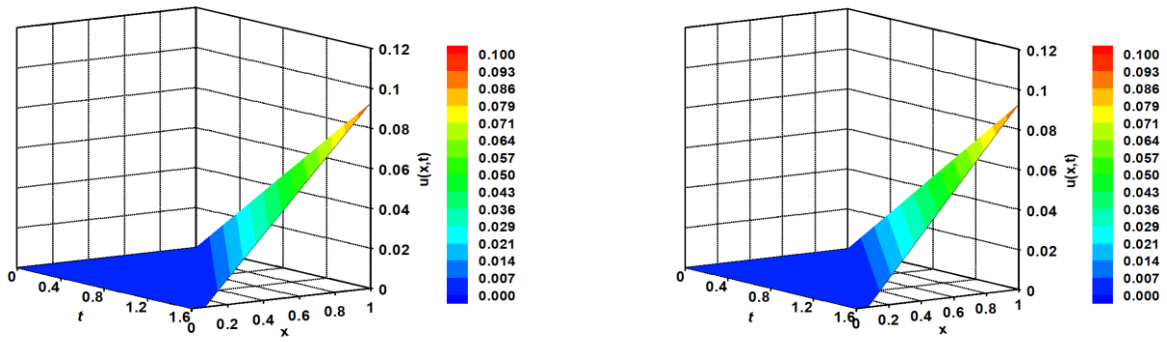

(a) (b)

Figure 7. Space-time evolution graph comparing numerical results (a) and analytical results (b) of $u(x,t)$ from t=0 to t = 1.6 s for test case 3

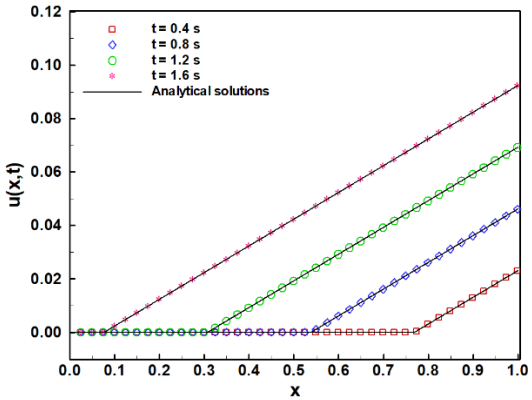

Figure 8. Comparison between numerical simulations (symbols) and analytical solutions (solid lines) of $u(x,t)$ at various times for test case 3

4. VALIDATION OF 2D WAVE EQUATION

In this section, three benchmark test cases are validated to verify the accuracy and efficiency of the proposed model for the 2D wave equation such as:

$$\frac{\partial^2 u}{\partial t^2} = c_s^2 \left(\frac{\partial^2 u}{\partial x^2} + \frac{\partial^2 u}{\partial y^2}\right), 0 \le x \le 1, 0 \le y \le 1, \quad 0 < t \quad (48)$$

The numerical results are compared with exact solutions for all test cases, including various initial and boundary conditions.

4. 1. 2D Sin-shaped Initial Condition (Slow Oscillation) (Test Case 4) The focus of this benchmark test case is to examine the 2D wave equation (Equation 48) with sinusoidal initial conditions as follows:

$$\begin{cases} u(x,y,0) = A\sin(kx)\sin(ky) \\ u_t(x,y,0) = 0 \end{cases} \quad (49)$$

where $k = \frac{2\pi}{\lambda}$ and $\lambda = 2$ for slow oscillation. The boundary conditions are:

$$\begin{cases} u(0,y,t) = u(1,y,t) = 0 \\ u(x,0,t) = u(x,1,t) = 0 \end{cases} \quad (50)$$

The analytical solution for this case can be found in literature as:

$$u(x,y,t) = A\sin(\pi x)\sin(\pi y)\cos(\sqrt{2}\pi c_s t) \quad (51)$$

where A denotes the amplitude of the wave. In this proceeding, it is adopted $\Delta x = \Delta y = 1 \times 10^{-3}$, $\Delta t = 5 \times 10^{-3}$, $c_s = 1.15$, $c = 2.0$.

Figure 9 compares a 9-bit 2D scheme (D2Q9) of the present model with an analytical solution extracted from Equation 51 for $u(x,y,t)$ at t= 3.2 s. For a clearer evaluation of the model accuracy, Figure 10 provides a 2D view of the comparison of numerical solutions (dashed red contours) and the analytical solutions (solid green contours). As shown in Figures 9 and 10, the numerical solutions have good agreement with the corresponding analytical solutions. Also, in the present test case, the errors of $u(x,y,t)$ are calculated and listed in Table 6. The table shows different standard errors, including E_2, E_∞, GRE, and RMS at particular times, namely, t=0.8 s, t=1.6 s, t=2.4 s, and t=3.2 s.

4. 2. 2D Sin-shaped Initial Condition (Fast Oscillation) (Test Case 5) The focus of this benchmark test case is to examine the 2D wave equation (Equation 48) with sinusoidal initial conditions as follows:

$$\begin{cases} u(x,y,0) = A\sin(kx)\sin(ky) \\ u_t(x,y,0) = 0 \end{cases} \quad (52)$$

where $k = \frac{2\pi}{\lambda}$ and $\lambda = 1$ for fast oscillation. The boundary conditions are:

$$\begin{cases} u(0,y,t) = u(1,y,t) = 0 \\ u(x,0,t) = u(x,1,t) = 0 \end{cases} \quad (53)$$

TABLE 5. Comparison of error norms E_2, E_∞, GRE, and RMS for $u(x,t)$ at various times for test case 3

t (s)	Error norms			
	E_2	E_∞	GRE	RMS
0.4	1.7033×10^{-3}	7.4652×10^{-5}	1.9152×10^{-3}	1.0944×10^{-5}
0.8	8.5511×10^{-4}	9.0556×10^{-5}	9.5543×10^{-4}	1.5515×10^{-5}
1.2	5.7116×10^{-4}	1.0116×10^{-4}	6.3581×10^{-4}	1.9027×10^{-5}
1.6	4.2889×10^{-4}	1.0922×10^{-4}	4.7631×10^{-4}	2.1992×10^{-5}

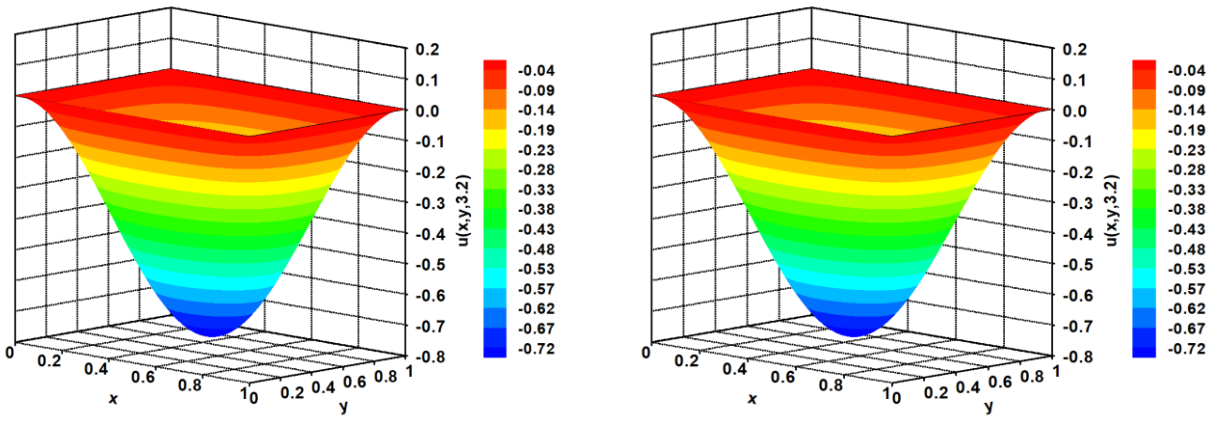

(a) (b)

Figure 9. Contour plots for the numerical results (a) and analytical results (b) of $u(x,y,t)$ at t = 3.2 s for test case 4

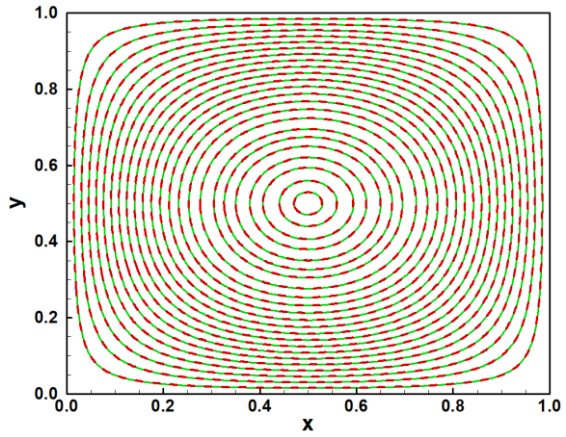

Figure 10. Comparison between numerical simulations (dashed red contours) and analytical solutions (solid green contours) of $u(x,y,t)$ at t=3.2 s for test case 4

The analytical solution for this case can be found in literature as:

$$u(x,y,t) = A\sin(2\pi x)\sin(2\pi y)\cos(\sqrt{8}\pi c_s t) \quad (54)$$

where A denotes the amplitude of the wave. In this proceeding, it is adopted $\Delta x = \Delta y = 1 \times 10^{-3}$, $\Delta t = 5 \times 10^{-3}$, $c_s = 1.15$, and $c = 2.0$.

Figure 11 compares a 9-bit 2D scheme (D2Q9) of the present model with an analytical solution extracted from Equation 54 for $u(x,y,t)$ at t= 3.2 s. For a clearer evaluation of the model accuracy, Figure 12 provides a 2D view of the comparison of numerical solutions (dashed red contours) and the analytical solutions (solid green contours). As seen in Figures 11 and 12, the numerical solutions have good agreement with the corresponding analytical solutions. Also, in the present test case, the errors of $u(x,y,t)$ are calculated and listed in Table 7. The table shows different standard errors, including E_2, E_∞, GRE, and RMS at particular times, namely, t=0.8 s, t=1.6 s, t=2.4 s, and t=3.2 s.

4. 3. Non-zero Initial Condition (Test Case 6)

The focus of this benchmark test case is to examine the 2D wave equation (Equation 48) with Non-zero initial conditions as follows:

$$\begin{cases} u(x,y,0) = \cos[2\pi f(-x\cos(\theta_0) - y\sin(\theta_0)] \\ u_t(x,y,0) = -2\pi f c_s \cdot \sin[2\pi f(-x\cos(\theta_0) - y\sin(\theta_0)] \end{cases} \quad (55)$$

and a time-depended boundary feed is provided by the non-zero Dirichlet boundary conditions as:

$$\begin{cases} u(0,y,t) = \cos[2\pi f(c_s t - y\sin(\theta_0)] \\ u(1,y,t) = \cos[2\pi f(c_s t - \cos(\theta_0) - y\sin(\theta_0)] \\ u(x,0,t) = \cos[2\pi f(c_s t - x\cos(\theta_0))] \\ u(x,1,t) = \cos[2\pi f(c_s t - x\cos(\theta_0) - \sin(\theta_0)] \end{cases} \quad (56)$$

The analytical solution for this equation can be found in literature (51) as:

$$u(x,y,t) = \cos[2\pi f(c_s t - x\cos(\theta_0) - y\sin(\theta_0)] \quad (57)$$

TABLE 6. Comparison of error norms E_2, E_∞, GRE, and RMS for $u(x, y,t)$ at various times for test case 4

t (s)	Error norms			
	E_2	E_∞	GRE	RMS
0.8	3.6839×10^{-3}	2.1051×10^{-3}	3.6839×10^{-3}	1.0515×10^{-3}
1.6	6.9491×10^{-3}	2.4111×10^{-3}	6.9491×10^{-3}	1.2044×10^{-3}
2.4	6.7069×10^{-4}	6.4920×10^{-4}	6.7069×10^{-4}	3.2427×10^{-3}
3.2	1.6013×10^{-4}	1.5984×10^{-4}	1.6013×10^{-4}	7.9837×10^{-5}

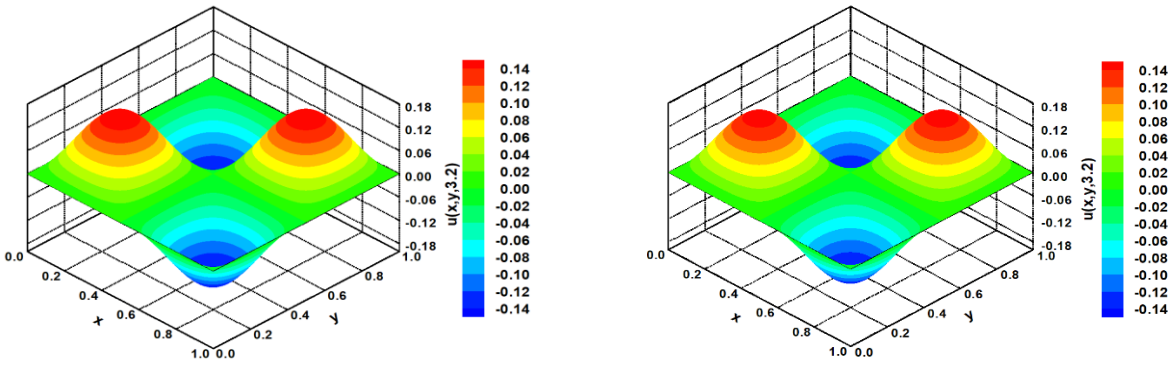

(a) (b)

Figure 11. Contour plots for the numerical results (a) and analytical results (b) of $u(x,y,t)$ at t = 3.2 s for test case 5

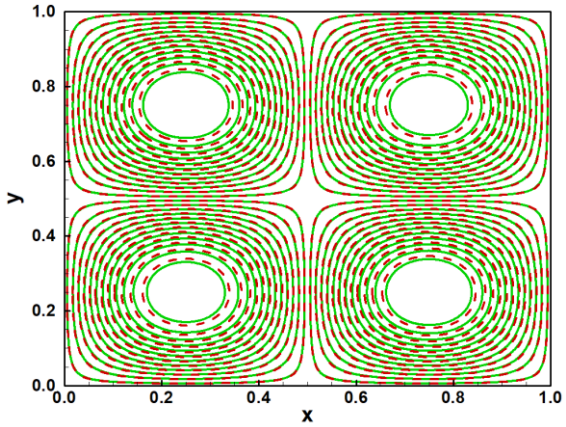

Figure 12. Comparison between numerical simulations (dashed red contours) and analytical solutions (solid green contours) of $u(x,y,t)$ at t=3.2 s for test case 5

where f denotes the frequency of the wave. In what follows, it is taken $\Delta x = \Delta y = 1 \times 10^{-3}$, $\Delta t = 5 \times 10^{-3}$, $c_s = 1.15$, $c = 2.0$, $\theta_0 = \frac{\pi}{2}$.

Figure 13 illustrates the comparison between a 9-bit 2D scheme (D2Q9) of the present model with an analytical solution extracted from Equation 57 for $u(x,y,t)$ at t= 3.2 s. For a clearer evaluation of the model accuracy, Figure 14 provides a 2D view of the comparison of numerical solutions (dashed red contours) and the analytical solutions (solid green contours). As seen in Figures 13 and 14, the numerical solutions have good agreement with the corresponding analytical solutions. Also, in the present test case, the errors of $u(x,y,t)$ are calculated and listed in Table 8. The table shows different standard errors, including E_2, E_∞, GRE, and RMS at particular times, namely, t=0.8 s, t=1.6 s, t=2.4 s, and t=3.2 s.

TABLE 7. Comparison of error norms E_2, E_∞, GRE, and RMS for $u(x,y,t)$ at various times for test case 5

t (s)	Error norms			
	E_2	E_∞	GRE	RMS
0.8	1.3929×10^{-2}	4.8331×10^{-3}	1.3929×10^{-2}	2.4141×10^{-3}
1.6	4.4154×10^{-3}	3.3523×10^{-3}	4.4154×10^{-3}	1.6745×10^{-3}
2.4	2.8983×10^{-3}	2.5327×10^{-3}	2.8983×10^{-3}	1.2650×10^{-3}
3.2	6.4944×10^{-4}	6.4466×10^{-4}	6.4944×10^{-4}	3.2200×10^{-4}

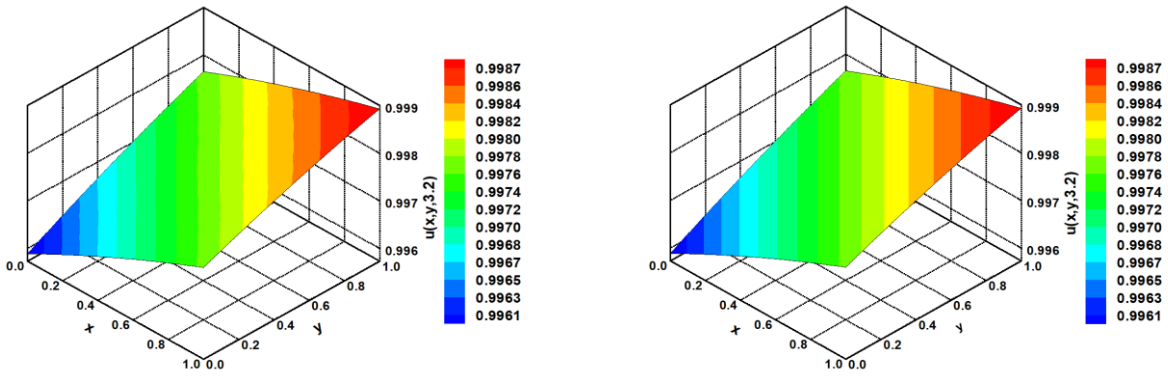

(a) (b)

Figure 13. Contour plots for the numerical results (a) and analytical results (b) of $u(x,y,t)$ at t = 3.2 s for test case 6

TABLE 8. Comparison of error norms E_2, E_∞, GRE, and RMS for $u(x,y,t)$ at various times for test case 6

t (s)	Error norms			
	E_2	E_∞	GRE	RMS
0.8	3.1652×10^{-4}	6.6069×10^{-4}	2.3789×10^{-4}	3.1646×10^{-4}
1.6	3.6448×10^{-4}	7.5794×10^{-4}	2.6939×10^{-4}	3.6374×10^{-4}
2.4	1.2629×10^{-4}	3.9020×10^{-4}	7.4887×10^{-5}	1.2548×10^{-4}
3.2	1.0779×10^{-4}	2.2890×10^{-4}	9.0200×10^{-5}	1.0647×10^{-4}

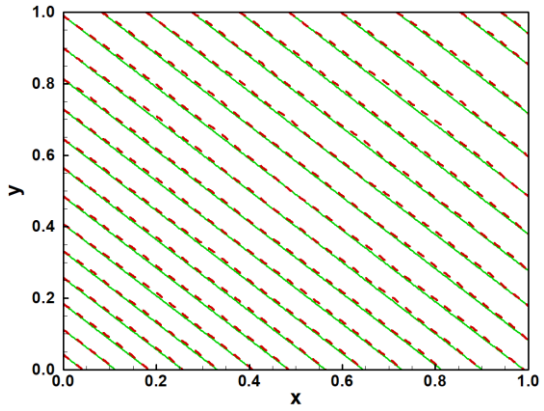

Figure 14. Comparison between numerical simulations (dashed red contours) and analytical solutions (solid green contours) of $u(x,y,t)$ at t=3.2 s for test case 6

5. CONCLUSION

In this paper, a lattice Boltzmann-adaptive model for solving the linear acoustic wave equation was introduced, employing a novel approach with a standard equilibrium distribution function featuring unknown coefficients. Through Chapman-Enskog analysis, the coefficients were determined, establishing a unique relationship for f_i^{eq} with a standard weighting factor across all lattice directions. Notably, the displacement of the wave, $u(\boldsymbol{x},t)$, was chosen as a zero-order macroscopic moment instead of $\partial u(\boldsymbol{x},t)/\partial t$, accurately recovering the macroscopic wave equation.

To validate the efficiency and accuracy of the present mesoscopic model, six test cases with varying initial and boundary conditions for both 1D and 2D problems were conducted. Utilizing a 3-bit scheme for 1D problems and a 9-bit scheme for 2D ones, in test case 1, errors range from 4.0888×10^{-6} to 1.1967×10^{-5} for t = 0.8- 3.2 seconds. Similarly, test case 2 exhibits errors ranging from 3.9618×10^{-5} to 4.0341×10^{-5} for t = 0.8- 3.2 seconds. For test case 3, errors range from 1.0944×10^{-5} to 2.1992×10^{-5} for t = 0.4- 1.6 seconds. Test case 4 shows errors ranging from 7.9837×10^{-5} to 3.2427×10^{-3} for t = 0.8- 3.2 seconds. In test case 5, errors range from 3.2200×10^{-4} to 1.2650×10^{-3} for t = 0.8- 3.2 seconds. Finally, test case 6 exhibits errors ranging from 1.0647×10^{-4} to $3.6374 \times 10^{-4}$for t = 0.8- 3.2 seconds. The numerical results demonstrated excellent agreement with analytical solutions, exhibiting a maximum error of 10^{-3} and a minimum error of 10^{-6}.

Furthermore, the accuracy test showed that the model possesses a spatial accuracy of second-order, with the slopes of the fitting lines in the relative error norm E_∞ plots being extremely close to 2 (1.964).

For future research, several avenues could develop the present adaptive model. Expanding the model to address three-dimensional problems, exploring its applicability to nonlinear acoustic wave equations, and investigating hybrid numerical techniques could lead to more efficient simulations.

6. REFERENCES

1. Mahnama S, Neshaei S, Mehrdad M, H Farahani M, Amanifard N. Simulation of gravity wave propagation in free surface flows by an incompressible SPH algorithm. International Journal of Engineering, Transactions A: Basics. 2012;25(3):239-48. 10.5829/idosi.ije.2012.25.03a.06
2. Ramli M. The deterministic generation of extreme surface water waves based on soliton on finite background in laboratory. 2009.
3. Dhuri DB, Hanasoge SM, Perlekar P, Robertsson JO. Numerical analysis of the lattice Boltzmann method for simulation of linear acoustic waves. Physical Review E. 2017;95(4):043306. 10.1103/PhysRevE.95.043306
4. Zomorodian R, Soltani F, Sivandi-Pour A, Noroozinejad Farsangi E. Effect of foundation flexibility on the seismic performance of a high-rise structure under far-field and near-field earthquakes. International Journal of Engineering, Transactions A: Basics. 2021;34(7):1611-22. 10.5829/ije.2021.34.07a.06
5. Javanrouh Givi R, Aminian Modarres A, Kafaee Razavi M. Investigating The Effects of Modem Electromagnetic Waves (2.4 GHz) on Electroencephalogram. International Journal of Engineering,Transactions B: Applications. 2019;32(8):1155-62. 10.5829/ije.2019.32.08b.11
6. Soltan A, Neshati M. Design and Development of High Gain, Low Profile and Circularly Polarized Cavity-backed Slot Antennas Using High-order Modes of Square Shaped Substrtae Integrated Waveguide Resonator. International Journal of Engineering, Transactions C: Aspects. 2017;30(12):1840-7. 10.5829/ije.2017.30.12c.04
7. Sun Y, Wu J, Li B. Rogue wave solutions of (3+ 1)-dimensional Kadomtsev-Petviashvili equation by a direct limit method. Communications in Theoretical Physics. 2023;75(6):065002. 10.1088/1572-9494/accb40
8. Li J, Fu Z, Gu Y, Zhang L. Rapid calculation of large-scale acoustic scattering from complex targets by a dual-level fast direct solver. Computers & Mathematics with Applications. 2023;130:1-9. 10.1016/j.camwa.2022.11.007
9. Ma X, Wang Y, Zhu X, Liu W, Lan Q, Xiao W. A spectral method for two-dimensional ocean acoustic propagation. Journal of Marine Science and Engineering. 2021;9(8):892. 10.3390/jmse9080892
10. Gander MJ, Halpern L, Rannou J, Ryan J. A direct time parallel solver by diagonalization for the wave equation. SIAM Journal on Scientific Computing. 2019;41(1):A220-A45. 10.1137/17M1148347
11. Ismael HF, Sulaiman TA. On the dynamics of the nonautonomous multi-soliton, multi-lump waves and their collision phenomena to a (3+ 1)-dimensional nonlinear model. Chaos, Solitons & Fractals. 2023;169:113213. 10.1016/j.chaos.2023.113213
12. Luo Y. Improved decay of solution for strongly damped nonlinear wave equations. Mathematical Biosciences and Engineering. 2023;20(3):4865-76. 10.3934/mbe.2023225
13. Jiao Z, Xu Y, Zhao L. Stability for nonlinear wave motions damped by time-dependent frictions. Communications in Nonlinear Science and Numerical Simulation. 2023;117:106965. 10.1016/j.cnsns.2022.106965
14. Naeem M, Yasmin H, Shah R, Shah NA, Nonlaopon K. Investigation of fractional nonlinear regularized long-wave

models via Novel techniques. Symmetry. 2023;15(1):220. 10.3390/sym15010220

15. Abdelkawy MA, Soluma E, Al-Dayel I, Baleanu D. Spectral solutions for a class of nonlinear wave equations with Riesz fractional based on Legendre collocation technique. Journal of Computational and Applied Mathematics. 2023;423:114970. 10.1016/j.cam.2022.114970
16. Mirbagheri S, RAJAEI T, MIRZAEI F. Solution of wave equations near seawalls by finite element method. 2008.
17. Akinyemi L, Şenol M, Iyiola OS. Exact solutions of the generalized multidimensional mathematical physics models via sub-equation method. Mathematics and Computers in Simulation. 2021;182:211-33. 10.1016/j.matcom.2020.10.017
18. Majid SZ, Faridi WA, Asjad MI, Abd El-Rahman M, Eldin SM. Explicit soliton structure formation for the riemann wave equation and a sensitive demonstration. Fractal and Fractional. 2023;7(2):102. 10.3390/fractalfract7020102
19. Ullah H, Islam S, Dennis L, Abdelhameed T, Khan I, Fiza M. Approximate solution of two-dimensional nonlinear wave equation by optimal homotopy asymptotic method. Mathematical Problems in Engineering. 2015;2015. 10.1155/2015/380104
20. Adwan M, Al-Jawary M, Tibaut J, Ravnik J. Analytic and numerical solutions for linear and nonlinear multidimensional wave equations. Arab Journal of Basic and Applied Sciences. 2020;27(1):166-82. 10.1080/25765299.2020.1751439
21. Jleli M, Kumar S, Kumar R, Samet B. Analytical approach for time fractional wave equations in the sense of Yang-Abdel-Aty-Cattani via the homotopy perturbation transform method. Alexandria Engineering Journal. 2020;59(5):2859-63. 10.1016/j.aej.2019.12.022
22. Wang W, Yan W, Yang D. A cell-centered finite volume scheme for the diffusive–viscous wave equation on general polygonal meshes. Applied Mathematics Letters. 2022;133:108274. 10.1016/j.aml.2022.108274
23. Chen L, Huang J, Fu L-Y, Peng W, Song C, Han J. A Compact High-Order Finite-Difference Method with Optimized Coefficients for 2D Acoustic Wave Equation. Remote Sensing. 2023;15(3):604. 10.3390/rs15030604
24. Farhadi A. Investigating the third order solitary wave generation accuracy using incompressible smoothed particle hydrodynamics. International Journal of Engineering, Transactions C: Aspects. 2016;29(3):426-35. 10.5829/idosi.ije.2016.29.03c.17
25. Wen P, Tao G, Spearot DE, Phillpot SR. Molecular dynamics simulation of the shock response of materials: A tutorial. Journal of Applied Physics. 2022;131(5). 10.1063/5.0076266
26. Doolen G. Lattice gas methods for partial differential equations: CRC Press; 2019.
27. Qin S, Jiang M, Ma K, Su J, Liu Z. Fully resolved simulations of viscoelastic suspensions by an efficient immersed boundary-lattice Boltzmann method. Particuology. 2023;75:26-49. 10.1016/j.partic.2022.06.004
28. Chen S, Doolen GD. Lattice Boltzmann method for fluid flows. Annual review of fluid mechanics. 1998;30(1):329-64. 10.1146/annurev.fluid.30.1.329
29. Chen R, Cao S, Liu W, Song Q, You Y. Acoustic multipole source–simplified lattice Boltzmann method for simulating acoustic propagation problems. International Journal for Numerical Methods in Fluids. 2023;95(7):1174-96. 10.1002/fld.5178
30. Burnside SB, Pasieczynski K, Zarareh A, Mehmood M, Fu YQ, Chen B. Simulations of surface acoustic wave interactions on a sessile droplet using a three-dimensional multiphase lattice Boltzmann model. Physical Review E. 2021;104(4):045301. 10.1103/PhysRevE.104.045301
31. Astoul T, Wissocq G, Boussuge J-F, Sengissen A, Sagaut P. Lattice Boltzmann method for computational aeroacoustics on non-uniform meshes: A direct grid coupling approach. Journal of Computational Physics. 2021;447:110667. 10.1016/j.jcp.2021.110667
32. Boolakee O, Geier M, De Lorenzis L. A new lattice Boltzmann scheme for linear elastic solids: periodic problems. Computer Methods in Applied Mechanics and Engineering. 2023;404:115756. 10.1016/j.cma.2022.115756
33. Qiu R-F, Che H-h, Zhou T, Zhu J-F, You Y-C. Lattice Boltzmann simulation for unsteady shock wave/boundary layer interaction in a shock tube. Computers & Mathematics with Applications. 2020;80(10):2241-57. 10.1016/j.camwa.2020.07.012
34. Hanasoge SM, Succi S, Orszag SA. Lattice Boltzmann method for electromagnetic wave propagation. Europhysics Letters. 2011;96(1):14002. 10.1209/0295-5075/96/14002
35. Qiu L-C, Tian L, Liu X-J, Han Y. A 3D multiple-relaxation-time LBM for modeling landslide-induced tsunami waves. Engineering Analysis with Boundary Elements. 2019;102:51-9. 10.1016/j.enganabound.2019.02.011
36. Kefayati G, Tolooiyan A, Dyson AP. Finite difference lattice Boltzmann method for modeling dam break debris flows. Physics of Fluids. 2023;35(1). 10.1063/5.0130947
37. DM C. Lattice BGK simulation of sound waves. 1998. 10.1209/epl/i1998-00346-7
38. Tan MK, Yeo LY. Hybrid finite-difference/lattice Boltzmann simulations of microchannel and nanochannel acoustic streaming driven by surface acoustic waves. Physical Review Fluids. 2018;3(4):044202. 10.1103/PhysRevFluids.3.044202
39. Chopard B, Luthi PO. Lattice Boltzmann computations and applications to physics. Theoretical Computer Science. 1999;217(1):115-30. 10.1016/S0304-3975(98)00153-4
40. Guangwu Y. A lattice Boltzmann equation for waves. Journal of Computational Physics. 2000;161(1):61-9. 10.1006/jcph.2000.6486
41. Zhang J, Yan G, Dong Y. A higher-order accuracy lattice Boltzmann model for the wave equation. International journal for numerical methods in fluids. 2009;61(6):683-97. 10.1002/fld.1981
42. Zhang J, Yan G, Shi X. Lattice Boltzmann model for wave propagation. Physical Review E. 2009;80(2):026706. 10.1103/PhysRevE.80.026706
43. Lai H, Ma C. Lattice Boltzmann model for generalized nonlinear wave equations. Physical Review E. 2011;84(4):046708. 10.1103/PhysRevE.84.046708
44. An B, Bergadà J. A 8-neighbor model lattice Boltzmann method applied to mathematical–physical equations. Applied Mathematical Modelling. 2017;42:363-81. 10.1016/j.apm.2016.10.016
45. Li D, Lai H, Shi B. Mesoscopic simulation of the (2+ 1)-dimensional wave equation with nonlinear damping and source terms using the lattice Boltzmann BGK model. Entropy. 2019;21(4):390. 10.3390/e21040390
46. Krüger T, Kusumaatmaja H, Kuzmin A, Shardt O, Silva G, Viggen EM, et al. The lattice Boltzmann equation. The Lattice Boltzmann Method: Principles and Practice. 2017:61-104. 10.1007/978-3-319-44649-3_3
47. Alizadeh A, Wang J, Pooyan S, Mirbozorgi S, Wang M. Numerical study of active control of mixing in electro-osmotic flows by temperature difference using lattice Boltzmann methods. Journal of colloid and interface science. 2013;407:546-55. 10.1016/j.jcis.2013.06.026
48. Nezhad JR, Mirbozorgi SA. An immersed boundary-lattice Boltzmann method to simulate chaotic micromixers with baffles.

Computers & Fluids. 2018;167:206-14. 10.1016/j.compfluid.2018.02.031

49. Shahriari A, Jahantigh N, Rakani F. Assessment of particle-size and temperature effect of nanofluid on heat transfer adopting lattice boltzmann model. International Journal of Engineering, Transactions A: Basics, . 2018;31(10):1749-59. 10.5829/ije.2018.31.10a.18

50. Tomlinson M, Tjhai CJ, Ambroze MA, Ahmed M, Jibril M. Error-correction coding and decoding: bounds, codes, decoders, analysis and applications: Springer Nature; 2017.

51. Yang D, Peng J, Lu M, Terlaky T. Optimal nearly analytic discrete approximation to the scalar wave equation. Bulletin of the Seismological Society of America. 2006;96(3):1114-30. 10.1785/0120050080

COPYRIGHTS

©2024 The author(s). This is an open access article distributed under the terms of the Creative Commons Attribution (CC BY 4.0), which permits unrestricted use, distribution, and reproduction in any medium, as long as the original authors and source are cited. No permission is required from the authors or the publishers.

Persian Abstract

چکیده

این مقاله به نیاز برای یک رویکرد کارآمد و سازگار برای حل معادلات موج صوتی خطی در روش شبکه بولتزمن (LBM) می‌پردازد. یک مدل جدید تطبیقی با شبکه معرفی شده است که از طریق تجزیه‌وتحلیل چاپمن-انسکوگ به دست آمده است که از یک رابطه واحد برای تابع توزیع تعادل در تمام ساختارهای شبکه استفاده می‌کند. استخراج مورد نظر با در نظر گرفتن یک تابع توزیع تعادل استاندارد با ضرایب مجهول آغاز می‌شود. با انتخاب جابجایی موج صوتی به‌عنوان ممان میکروسکوپی مرتبه صفر، بازیابی دقیق معادله موج ماکروسکوپی تضمین می‌شود. برخلاف روش‌های موجود، این مدل پیچیدگی مرتبط با روابط توابع توزیع تعادلی را ساده می‌کند و تطبیق‌پذیری بیشتری را ارائه می‌دهد. این مدل از طریق مقایسه با مسایل معیار گسترده روی انتشار موج یک‌بعدی و دوبعدی تأیید می‌شود. نتایج نشان‌دهنده تطابق عالی با راه‌حل‌های تحلیلی، با حداکثر میانگین مربع خطاهای 10^{-3} (٪۰/۱ >خطا) و حداقل میانگین مربع خطاهای 10^{-6} (٪۰/۰۰۰۱> خطا)، نشان‌دهنده دقت پیش‌بینی بالا (٪۹۹/۹<)است. علاوه بر این، مدل حاضر دقت مکانی مرتبه دوم را نشان می‌دهد، با معیار خطای نسبی E_2 که شیب‌های نزدیک به ۲ را نشان می‌دهد که نشان‌دهنده دقت مکانی مرتبه دوم است. هم‌چنین شبیه‌سازی‌های عددی کاهش خطای مذکور را برای اندازه شبکه ریزتر نشان می‌دهند.